Original Article

Assessment of Imaging Findings of Renal Carcinoma Subtypes with 3.0T MRI

MO Nalbant, E Inci

Department of Radiology, University of Health Sciences, Bakirkoy Dr. Sadi Konuk Training and Research Hospital, Istanbul, Turkey

Abstract

Background: The prevalence of renal masses has escalated as a result of the augmented utilization of cross-sectional imaging techniques. The approach to managing renal masses may exhibit variability contingent upon the subtype of renal cell carcinoma (RCC). **Aim:** This research aimed to distinguish between clear cell and papillary RCCs, utilizing dynamic contrast magnetic resonance imaging (MRI) and diffusion-weighted imaging (DWI). **Materials and Methods:** The study assessed the MR images of 112 patients with RCC. Two radiologists independently analyzed tumor size, vascular involvement, signal characteristics in T1- and T2-weighted sequences, the presence of hemosiderin, both microscopic and macroscopic fat content, enhancement patterns, and apparent diffusion coefficient (ADC) values derived from b-values of 1000 s/mm². **Results:** Seventy patients had clear cell RCC, and 42 had papillary. In the clear cell RCC, microscopic fat content was significantly higher than the papillary RCC ($P < 0.001$). However, in papillary RCC, hemosiderin content was substantially greater ($P = 0.001$). On T2-weighted MR images, clear cell RCCs were usually hyperintense, while papillary RCCs were hypointense ($P < 0.001$). Even though the rapid enhancement pattern was observed in clear cell RCCs, the progressive enhancement pattern was more prevalent in papillary RCCs ($P < 0.001$). **Conclusion:** Hyperintensity on T2-weighted images, microscopic fat content, and rapid enhancement pattern may be indicative of clear cell RCC, whereas hypointensity on T2-weighted images, hemosiderin content, and a progressive contrast pattern may be diagnostic for papillary RCC.

Keywords: *Apparent diffusion coefficient, clear cell renal cell carcinoma, hemosiderin, magnetic resonance imaging, microscopic fat, papillary renal cell carcinoma*

Received: 16-May-2023; **Revision:** 20-Jun-2023; **Accepted:** 06-Jul-2023; **Published:** 04-Dec-2023

Introduction

The frequency of incidental solid renal masses has grown due to the increased use of cross-sectional imaging.[1] The condition exhibits a mortality rate ranging from 30% to 40% and displays a higher incidence in males as compared to females. Apart from gender, RCC is associated with additional risk factors such as obesity, hypertension, smoking, and chronic kidney disease.[2,3] The three most prevalent subtypes of RCC are clear cell RCC, papillary RCC, and chromophobe RCC.[4,5] With a 5-year survival rate of 44%–69%, clear cell carcinomas have a poorer prognosis than the other subtypes.[6-9]

The management of renal masses may vary depending on the subtype of RCC. They respond differently to molecularly targeted therapy. Clear cell RCCs respond to tyrosine kinase inhibitors. However, the rapamycin inhibitor (temsirolimus) is more effective for treating nonclear cell RCCs.[10,11] For therapeutic regimens, it is essential to know the precise subtype of the RCC before

Access this article online	
Quick Response Code:	Website: www.njcponline.com
	DOI: 10.4103/njcp.njcp_373_23

Address for correspondence: Dr. MO Nalbant, Department of Radiology, University of Health Sciences, Bakirkoy Dr. Sadi Konuk Training and Research Hospital, Tevfik Saglam Cad. No. 11 Zuhuratbaba, Bakirkoy, Istanbul - 34147, Turkey. E-mail: musnalbant88@hotmail.com

How to cite this article: Nalbant MO, Inci E. Assessment of imaging findings of renal carcinoma subtypes with 3.0T MRI. Niger J Clin Pract 2023;26:1750-7.

treatment. A biopsy can be used to diagnose solid renal masses histopathologically. Nevertheless, it can cause complications such as hemorrhage, requiring the use of noninvasive cross-sectional imaging.[12]

Due to the variability of imaging properties and the convergence of imaging features, the absence of effective imaging criteria for distinguishing RCC subtypes remains a difficulty. Multiparametric magnetic resonance imaging (MRI) is a valuable noninvasive method for the detection and evaluation of renal masses because of its substantial soft-tissue contrast that enables the characterization of lesions' contrast enhancement pattern, microscopic or macroscopic fat content, and restriction of diffusion. This technique might aid in the classification of RCC subtypes. Clear cell RCC may be indicated by hyperintensity on T2-weighted images, microscopic lipid content, and a rapid enhancement pattern, whereas papillary RCC may be indicated by hypointensity on T2-weighted images, hemosiderin content, and a progressive contrasting pattern. In our study, we aimed to determine the diagnostic utility of multiparametric MRI in identifying and differentiating the most prevalent RCC subtypes.

Materials and Methods

Study population

This retrospective research was authorized by the Ethics Committee of our university (approval number: 2023/95) and examined patients with RCC whose diagnosis was verified histologically following surgery from June 2016 to February 2023. The study's inclusion criteria were as follows: (a) patients who underwent multiparametric 3T abdomen MRI before surgery; (b) patients with no invasive procedures carried out before the operation; (c) patients surgically confirmed to have RCC; (d) patients with clear cell or papillary RCC verified histopathologically.

The search resulted in the identification of 337 patients. 52 patients treated at other hospitals, 107 patients without a 3.0T MRI examination, 28 patients who underwent presurgical invasive procedures, 13 patients whose image quality was not optimal for evaluation due to artifacts, and 21 patients with pathological subtypes other than RCC (ten patients with angiomyolipoma, eight patients with renal oncocytoma, and three patients with metastasis) were omitted from this research. Only four of the remaining 116 patients had chromophobe RCC. Due to the small sample size, these patients were excluded from the study. Finally, the study comprised a total of 112 patients (70 with clear cell RCC and 42 with papillary RCC), including 73 males and 39 females. The interval between the MRI and the operation varied between 7 and 14 days.

MRI examination

A 3.0-T MR unit (Verio; Siemens Medical Solutions, Erlangen, Germany) with a 16-channel phased array surface coil for signal reception was utilized for the examination. The imaging sequences included T2-weighted Half-Fourier Acquisition Single-Shot Turbo Spin Echo (HASTE) images in the transverse and coronal planes (25 slices; thickness: 3 mm with no intersection gap; TR/TE: 1000/95 ms; number of signals acquired: 2; voxel size: 1.2 × 1.2 × 4 mm), T1-weighted volumetric interpolated breath-hold examination (VIBE)-Dixon images in the transverse plane (30 slices; thickness: 3 mm with no intersection gap; TR/TE: 4.15/1.36 ms; number of signals acquired: 2; voxel size: 1.2 × 1.2 × 3 mm) (reconstruction of fat, water in phase and opposed-phase images acquired before and after contrast during cortico-medullary, early nephrographic, and late nephrographic phases). For diffusion-weighted imaging (DWI), respiratory-triggered single-shot echo-planar sequences were performed in the axial plane [matrix, 160 × 192; FOV, 36–44 cm; slice thickness, 4 mm; intersection gap, 1 mm; bandwidth, 250 kHz/pixel; acquisition time, 4–5 min; flip angle, 90°; number of excitations (NEX), 6] and images were acquired at b-values of 1000 s/mm^2.

Image analysis

Two radiologists with between nine and seventeen years of experience interpreting abdominal MRI scans evaluated MRI images separately. All patients were diagnosed with RCC; however, the histological subtype of the tumor was unknown to the researchers.

On axial T2-weighted sequences, the mean tumor size was measured. Vascular involvement was considered when renal vein invasion was present. Using T2-weighted HASTE and non-contrast T1-weighted VIBE-Dixon images, signal characteristics in the renal mass were evaluated only in the enhancing areas of the lesion. Analysis of post-contrast images allowed an accurate evaluation of the renal tumor's enhancing portions. The signal intensity was classified as hypointense, isointense, or hyperintense relative to the renal cortex.

On opposed-phase images, a distinct decrease in signal intensity compared to in-phase images at the identical anatomic location is regarded as conclusive evidence of microscopic fat in a renal mass.[13] When the subjective evaluation was inconclusive, a quantitative evaluation utilizing a region of interest (ROI) was attempted. The presence of microscopic fat was ascertained by comparing the signal intensity within an ROI located within the mass on in-phase images to the signal intensity within the same ROI on

opposed-phase images. If the former was greater than the sum of the standard deviation of the ROI measurements on both in-phase and opposed-phase images, then the presence of microscopic fat was confirmed. The assessment of hemosiderin involved a comparison of signal intensity between in-phase imaging and opposed-phase imaging, with a focus on the susceptibility effect resulting in decreased signal intensity.[14] The evaluation of macroscopic fat presence in the lesion was conducted by assessing fat-suppressed T1-weighted sequences alongside in-phase and opposed-phase sequences.

The enhancement pattern was classified into two groups: rapid enhancement (which peaked during the cortico-medullary or nephrographic phase) and progressive enhancement (which peaked in the delayed phase). The identification of significant enhancement was confidently established through visual examination. To perform a quantitative evaluation of heterogeneous tumors, a region of interest (ROI) measuring approximately 100 mm^2 was positioned within the tumor region exhibiting the highest degree of intense contrast enhancement, as determined by visible evaluation.

The minimum ADC value (ADCmin), mean ADC value (ADCmean), and maximum ADC value (ADCmax) were also assessed. The analysis of signal intensity in apparent diffusion coefficient (ADC) mapping is limited to the enhancing components of the masses, and cystic or necrotic areas were ruled out of the renal mass. For each lesion, a ROI was carefully formed on the ADC map to include as much of the lesion as possible [Figure 1].

Statistical analysis

With the assistance of the SPSS 25.0 software, statistical analyses were conducted. Using histograms and the Kolmogorov–Smirnov test, the conformance of the variables to the normal distribution was determined. Mean, standard deviation, median, and interquartile range (IQR) values were utilized for presenting descriptive statistics. The Pearson Chi-squared test was utilized to evaluate the association between categorical variables. The Mann–Whitney U test was used to compare non-normally distributed (nonparametric) variables between two groups. Instances with a P value of less than 0.05 were regarded as statistically significant.

Results

Patients

Our research included 112 patients. 70 patients (49 males, 21 females) were characterized as having clear cell RCC, and 42 patients (24 males, 18 females) were identified as having papillary RCC based on histopathology. The mean ages of the two groups were 56.16 ± 13.04 and 54.14 ± 10.91, respectively. Gender (P = 0.167) and age (P = 0.482) were not significantly different among the two subgroups.

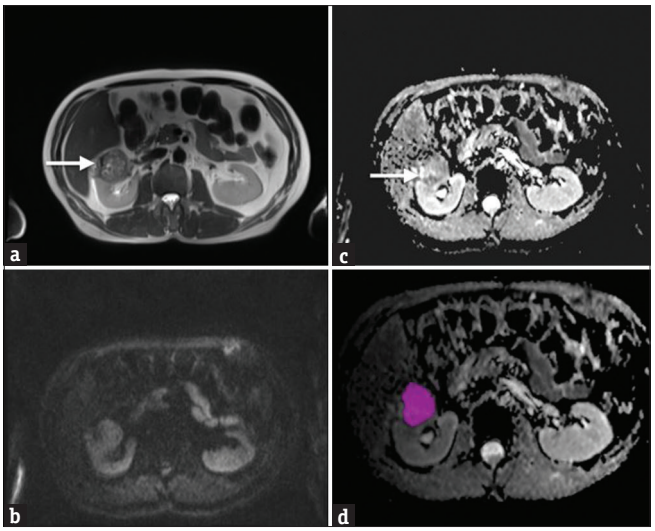

Figure 1: An example of a manually generated ROI for analyzing ADC values on the ADC map. The lesion was hypointense on the axial T2W (a) (white arrow) and hyperintense on the DW image (b) It was hypointense on the ADC sequence. These sequences were referenced for specifics, and cystic areas inside the lesion were not evaluated (white arrow) (c) Thus, the ROI was placed on the ADC map (d)

Interobserver agreement

The level of agreement between the two observers was assessed with the interclass correlation coefficient (ICC) or Cohen's kappa. Except for the difference in T1 signal intensity compared to the kidney (kappa value of 0.73), both the ICCs and the kappa values were above 0.8, showing that there was almost perfect agreement [Table 1].

Image analysis

In the clear cell RCC group, the mean diameter of the tumor was 57.97 ± 33.50 mm, whereas the mean diameter of the tumor in the papillary RCC group was 41.57 ± 27.24 mm. The clear cell RCC group had a larger mean tumor diameter than the papillary RCC group (P = 0.047).

The evaluation of MR image characteristics revealed a substantial difference between the microscopic fat and hemosiderin content of the masses. 43 (61.4%) of 70 clear cell RCCs and 6 (14.3%) of 42 papillary RCCs had microscopic fat, and the difference was statistically significant (P < 0.001) [Figure 2]. The sensitivity of the microscopic fat content was 72.8%, and the specificity was 98.2%. 18 (42.9%) of 42 papillary RCCs and 8 (11.4%) of 70 clear cell RCCs

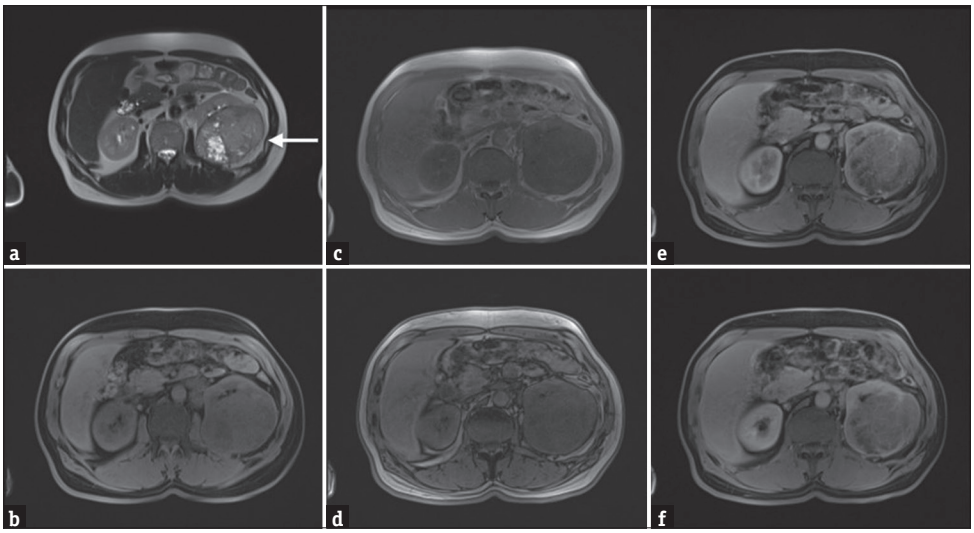

Figure 2: Clear cell renal cell carcinoma in a 56-year-old woman. The lesion was heterogeneous, hyperintense on the axial T2W image (a) (white arrow) and hypointense on the axial fat-suppressed T1W image (b) The observation of hyperintensity in the in-phase series (c) and hypointensity in the opposed-phase series (d) was compatible with the presence of microscopic fat. In the contrast-enhanced sequences, mild wash-out was observed (e and f)

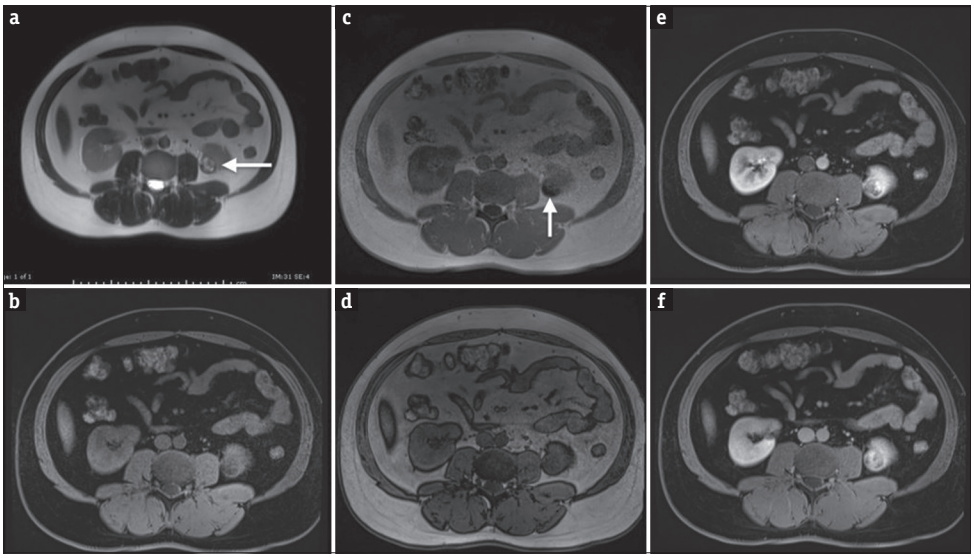

Figure 3: Papillary renal cell carcinoma in a 39-year-old man. Axial T2W (a) (white arrow) and fat-suppressed T1W (b) Images show heterogeneous signal intensity. In the in-phase (c) Opposed-phase (d) Series, hypointensity (white arrow) due to hemosiderin content was observed. In the contrast-enhanced sequences, progressive enhancement was observed (e and f)

Table 1: MRI image features' kappa values for lesions measured by two observers

Magnetic resonance imaging features	Weighted kappa	Level of agreement
Microscopic fat content	0.91	Almost perfect
Macroscopic fat content	0.85	Almost perfect
Hemosiderin content	0.82	Almost perfect
Vascular involvement	0.96	Almost perfect
Enhancement pattern	0.94	Almost perfect
T1 signal intensity compared to the renal cortex	0.73	Substantial
T2 signal intensity compared to the renal cortex	0.89	Almost perfect

had hemosiderin [Figure 3]. The difference was quantitatively substantial (P = 0.001) [Table 2]. The hemosiderin content had a sensitivity of 71.1% and a specificity of 94.9%.

1 (2.4%) of 42 papillary RCCs and 4 (5.7%) of 70 clear cell RCCs had macroscopic fat; the difference was not significant (P = 0.408). Vascular involvement was observed in 12 (17.1%) of 70 clear cell RCCs

Table 2: Comparison of papillary and clear cell renal cell carcinoma findings

		Papillary RCC *n* (%)/mean±s.d.	Clear cell RCC *n* (%)/mean±s.d.	*P*
Age		54.14±10.91	56.16±13.04	0.482[a]
Sex	Male	24 (57.1)	49 (70.0)	0.167[b]
	Female	18 (42.9)	21 (30.0)	
Tumor diameter (mm)		41.57±27.24	57.97±33.50	0.047[a]
Microscopic fat	Absent	36 (85.7)	27 (38.6)	<0.001[b]
	Present	6 (14.3)	43 (61.4)	
Macroscopic fat	Absent	41 (97.6)	66 (94.3)	0.408[b]
	Present	1 (2.4)	4 (5.7)	
Hemosiderin	Absent	24 (57.1)	62 (88.6)	0.001[b]
	Present	18 (42.9)	8 (11.4)	
Vascular involvement	Absent	37 (88.1)	58 (82.9)	0.454[b]
	Present	5 (11.9)	12 (17.1)	
Enhancement pattern	Rapid	5 (11.9)	52 (74.3)	<0.001[b]
	Progressive	37 (88.1)	18 (25.7)	
T1 signal intensity compared to the renal cortex	Hyperintense	7 (16.7)	12 (17.1)	0.593[b]
	Hypointense	8 (19.0)	19 (27.2)	
	Isointense	27 (64.3)	39 (55.7)	
T2 signal intensity compared to the renal cortex	Hyperintense	6 (14.3)	55 (78.6)	<0.001[b]
	Hypointense	34 (80.9)	10 (14.3)	
	Isointense	2 (4.8)	5 (7.1)	

RCC=Renal cell carcinoma. [a]Mann–Whitney *U* Test; [b]Chi-squared test

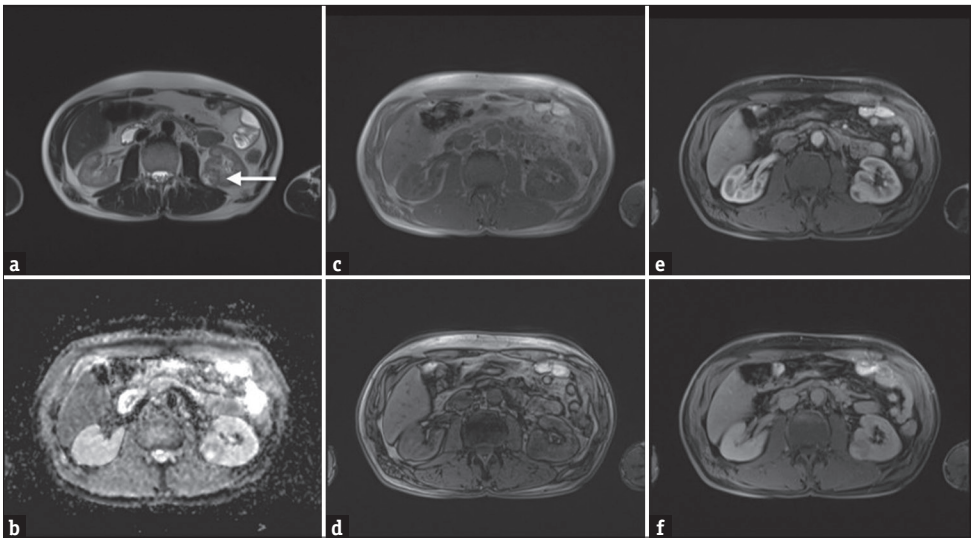

Figure 4: Clear cell renal cell carcinoma in a 57-year-old man. The lesion was hyperintense on T2W sequences (a) (white arrow) and the apparent diffusion coefficient image showed hypointensity consistent with diffusion restriction (b) Hyperintensity in the in-phase series (c) and hypointensity in the opposed-phase series (d) were observed, which was consistent with microscopic fat content. In the contrast-enhanced sequences, the arterial phase (e) shows rapid enhancement of the mass and wash-out in the delayed phase (f)

and 5 (11.9%) of 42 papillary RCCs. There was no statistically noteworthy difference ($P = 0.454$) [Table 2].

On T2-weighted MR images, 55 (78.6%) of 70 clear cell RCCs were hyperintense, whereas 6 (14.3%) of 42 papillary RCCs were hyperintense in comparison to the renal cortex. The masses of 34 (80.9%) patients with papillary RCC and 10 (14.3%) patients with clear cell RCC were hypointense compared to the renal cortex [Figures 4 and 5]. With 87.5% sensitivity and 95.3% specificity, the difference was statistically significant ($P < 0.001$) [Table 2].

On T1-weighted MR images, 27 (64.3%) of 42 papillary RCCs and 39 (55.7%) of 70 clear cell RCCs were isointense compared to the renal cortex. Compared to the renal cortex, the masses of 8 (19.0%) patients with papillary RCC and 19 (27.2%) patients with clear cell RCC were hypointense. The signal intensity on T1-weighted MR

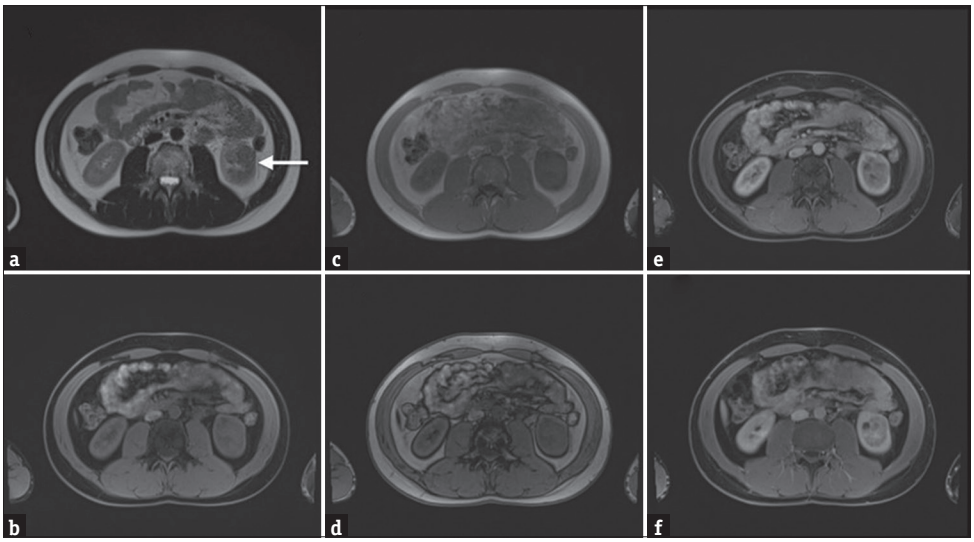

Figure 5: Papillary renal cell carcinoma in a 25-year-old man. The lesion was hypointense on axial T2W (a) (white arrow) and fat-suppressed T1W (b) images. In the in-phase (c) and opposed-phase (d) series, no findings related to fat content were detected. In the contrast-enhanced sequences, the mass is not significantly enhanced in the arterial phase (e) but progressively enhanced in the delayed phase (f)

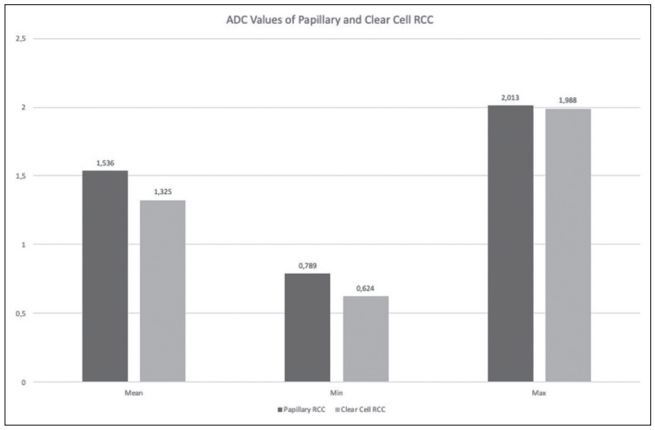

Figure 6: ADC values of papillary renal cell carcinomas and clear cell renal cell carcinomas are seen. Apparent diffusion coefficient values are expressed as × 10^{-3} mm²/s

images did not vary substantially between the two RCC subtypes (P = 0.593) [Table 2].

When assessing the enhancement characteristic of the RCCs, 52 (74.3%) of 70 clear cell RCCs peaked in the cortico-medullary or nephrographic phase, and 37 (88.1%) of 42 papillary RCCs peaked in the delayed phase, which was statistically significant between the two groups (P < 0.001) [Figures 4 and 5]. The sensitivity was 87.5%, and the specificity was 95.3% [Table 2].

The ADCmin (0.789 × 10^{-3} mm²/s in the papillary RCCs, 0.624 × 10^{-3} mm²/s in the clear cell RCCs), ADCmean (1.536 × 10^{-3} mm²/s in the papillary RCCs, 1.325 × 10^{-3} mm²/s in the clear cell RCCs), and ADCmax (2.013 × 10^{-3} mm²/s in the papillary RCCs, 1.988 × 10^{-3} mm²/s in the clear cell RCCs) values of the papillary RCCs were all higher than those of the clear cell RCCs; however, the difference was not statistically significant. The P values were 0.412, 0.173, and 0.626, respectively [Figure 6].

Discussion

In this study, the diagnostic significance of multiparametric 3T MRI was assessed for distinguishing clear cell RCC from papillary RCC. Recent studies have demonstrated that clear cell RCC often exhibits high signal intensity in T2-weighted images, a propensity for heterogeneity due to necrosis, cystic degeneration, or bleeding, and hypo- to isointense signal intensity in T1-weighted images.[15] They were found to frequently exhibit heterogeneous enhancement during the arterial phase and enhance more rapidly than other RCC subtypes, which is a distinguishing characteristic amongst RCC subtypes. Clear cell carcinomas are further distinguished by the presence of intralesional microscopic fat, which may present as a loss of signal intensity on opposed-phase MRI sequences.[16-18] Our research revealed a statistically significant increase in microscopic fat content and hyperintensity on T2-weighted images in the clear cell RCC subtype, which is consistent with prior investigations. Clear cell RCCs tend to infiltrate blood vessels, most often the renal vein and inferior vena cava. Hence, the examination of vascular involvement is crucial.[19] However, no significant disparity was detected in vascular involvement between the two subtypes in our investigation.

Papillary RCCs frequently exhibit regions of cystic degeneration, hemorrhage, and necrosis.[20] They often have low T2 signal intensity and hypovascularity

with progressive enhancement after contrast material injection, according to previous research,[21,22] and may include hemosiderin, causing signal loss on in-phase images compared to opposed-phase images in MRI imaging which was consistent with our study.

In addition, we investigated the contrast enhancement features of RCCs by measuring the signal intensity throughout various stages of multiparametric MRI and found that clear cell RCCs peaked in the cortico-medullary or nephrographic phase, whereas papillary RCCs peaked in the delayed phase. Similar to our study, Campbell *et al*. revealed that papillary RCC enhances less than the renal parenchyma in the early phases and exhibits gradual progressive enhancement, while clear cell RCC enhances more than the parenchyma during the cortico-medullary phase and shows wash-out during the late phases.[23] Chandarana *et al*.[24] observed that the cortico-medullary phase contrast enhancement ratio may distinguish clear cell RCC from papillary RCC with 90.9% sensitivity and 84.2% specificity. Sun *et al*.[25] reported the greatest variation in signal intensity was in early-phase images. Comparing clear cell RCCs to nonclear cell RCCs as a whole, Serter *et al*.[26] observed an important difference in contrast enhancement ratio values in the venous phase only.

Similar to what we reported, Outwater *et al*. and Karlo *et al*. found that in clear cell RCC, as opposed to nonclear cell RCC, a visible reduction in signal intensity on opposed-phase series was detected substantially more often.[18,27]

Previous research has identified the presence of intralesional macroscopic fat in a subset of RCCs with clear cell differentiation. However, this is not a subtype-specific finding, as papillary RCC may rarely include fat.[28] In our research, macroscopically substantial fat was not observed in RCCs.

In our study, clear cell RCC had lower ADC values than papillary RCC, although the difference was not statistically significant. Chen *et al*.[29] observed that the median ADC value for clear cell RCC was 1.67×10^{-3} mm^2/s, while for nonclear cell RCC it was 3.67×10^{-3} mm^2/s. According to different research, ADC signals with clear cell RCC were considerably lower.[30] On the contrary, Li *et al*.[31] found that nonclear cell RCC had lower ADC values than clear cell RCC, and the majority of samples with ADC values $<1.42 \times 10^{-3}$ mm^2/s were nonclear cell RCC. This may be due to the patient cohort of the study. Long illness progression and substantial tumor growth were characteristics of the selected cases in their research. Large tumors are susceptible to cystic transformation, which can lead to higher ADC values in patients with clear cell carcinoma.

Our study had several limitations. We were unable to include cases of chromophobe cell carcinoma since we had just four cases. This may be because of their relatively low frequency; nevertheless, larger-scale investigations are necessary to confirm these observations. Patients whose mass was too advanced for resection were omitted. Due to the retrospective nature of our study, selection bias was unavoidable despite the use of strict criteria for inclusion. We did not evaluate the correlation between imaging and histology features of RCCs. The distribution of enhancement was determined by the tumor's differentiation level and was associated with many alterations in its histology.

In conclusion, in MRI scans conducted with the preliminary diagnosis of renal mass, hyperintensity on T2-weighted images, microscopic fat content, and a rapid enhancement pattern may indicate clear cell RCC, while hypointensity on T2-weighted images, hemosiderin content, and a progressive contrasting pattern may suggest papillary RCC.

Acknowledgment

There are no known conflicts of interest associated with this publication. This research did not receive any specific grant from funding agencies in the public, commercial, or not-for-profit sectors. All of the authors declare that they have all participated in the design, execution, and analysis of the paper and that they have approved the final version. Written informed consent was obtained from all patients.

Financial support and sponsorship

Nil.

Conflicts of interest

There are no conflicts of interest.

References

1. Laguna MP, Algaba F, Cadeddu J, Clayman R, Gill I, Gueglio G, *et al*. Current patterns of presentation and treatment of renal masses: A clinical research office of the endourological society prospective study. J Endourol 2014;28:861-70.
2. Wang W, Cao K, Jin S, Zhu X, Ding J, Peng W. Differentiation of renal cell carcinoma subtypes through MRI-based radiomics analysis. Eur Radiol. 2020;30:5738-47.
3. Bahadoram S, Davoodi M, Hassanzadeh S, Bahadoram M, Barahman M, Mafakher L. Renal cell carcinoma: An overview of the epidemiology, diagnosis, and treatment. G Ital Nefrol 2022;39:2022-vol3.
4. Truong LD, Shen SS. Immunohistochemical diagnosis of renal neoplasms. Arch Pathol Lab Med 2011;135:92-109.
5. Bhandari A, Ibrahim M, Sharma C, Liong R, Gustafson S, Prior M. CT-based radiomics for differentiating renal tumours: A systematic review. Abdom Radiol (NY). 2021;46:2052-63.

6. Ramamurthy NK, Moosavi B, McInnes MD, Flood TA, Schieda N. Multiparametric MRI of solid renal masses: Pearls and pitfalls. Clin Radiol 2015;70:304-16.
7. Choi YA, Kim CK, Park SY, Cho SW, Park BK. Subtype differentiation of renal cell carcinoma using diffusion-weighted and blood oxygenation level-dependent MRI. AJR Am J Roentgenol 2014;203:W78-84.
8. Gurel S, Narra V, Elsayes KM, Siegel CL, Chen ZE, Brown JJ. Subtypes of renal cell carcinoma: MRI and pathological features. Diagn Interv Radiol 2013;19:304-11.
9. Hötker AM, Karlo CA, Zheng J, Moskowitz CS, Russo P, Hricak H, *et al*. Clear cell renal cell carcinoma: Associations between CT features and patient survival. AJR Am J Roentgenol 2016;206:1023-30.
10. Armstrong AJ, Halabi S, Eisen T, Broderick S, Stadler WM, Jones RJ, *et al*. Everolimus versus sunitinib for patients with metastatic non-clear cell renal cell carcinoma (ASPEN): A multicentre, open-label, randomised phase 2 trial. Lancet Oncol 2016;17:378-88.
11. Fernández-Pello S, Hofmann F, Tahbaz R, Marconi L, Lam TB, Albiges L, *et al*. A systematic review and meta-analysis comparing the effectiveness and adverse effects of different systemic treatments for non-clear cell renal cell carcinoma. Eur Urol 2017;71:426-36.
12. Capitanio U, Larcher A, Fallara G, Trevisani F, Porrini E, Di Marco F, *et al*. Parenchymal biopsy in the management of patients with renal cancer. World J Urol 2021;39:2961-8.
13. Schieda N, Davenport MS, Pedrosa I, Shinagare A, Chandarana H, Curci N, *et al*. Renal and adrenal masses containing fat at MRI: Proposed nomenclature by the society of abdominal radiology disease-focused panel on renal cell carcinoma. J Magn Reson Imaging 2019;49:917-26.
14. Childs DD, Clingan MJ, Zagoria RJ, Sirintrapun J, Tangtiang K, Anderson A, *et al*. In-phase signal intensity loss in solid renal masses on dual-echo gradient-echo MRI: Association with malignancy and pathologic classification. AJR Am J Roentgenol 2014;203:W421-8.
15. Muglia VF, Prando A. Renal cell carcinoma: Histological classification and correlation with imaging findings. Radiol Bras 2015;48:166-74.
16. Hötker AM, Mazaheri Y, Wibmer A, Karlo CA, Zheng J, Moskowitz CS, *et al*. Differentiation of clear cell renal cell carcinoma from other renal cortical tumors by use of a quantitative multiparametric MRI approach. AJR Am J Roentgenol 2017;208:W85-91.
17. Pedrosa I, Sun MR, Spencer M, Genega EM, Olumi AF, Dewolf WC, *et al*. MR imaging of renal masses: Correlation with findings at surgery and pathologic analysis. Radiographics 2008;28:985-1003.
18. Karlo CA, Donati OF, Burger IA, Zheng J, Moskowitz CS, Hricak H, *et al*. MR imaging of renal cortical tumours: Qualitative and quantitative chemical shift imaging parameters. Eur Radiol 2013;23:1738-44.
19. Bissada NK, Yakout HH, Babanouri A, Elsalamony T, Fahmy W, Gunham M, *et al*. Long-term experience with management of renal cell carcinoma involving the inferior vena cava. Urology 2003;61:89-92.
20. Prasad SR, Humphrey PA, Catena JR, Narra VR, Srigley JR, Cortez AD, *et al*. Common and uncommon histologic subtypes of renal cell carcinoma: Imaging spectrum with pathologic correlation. Radiographics 2006;26:1795-806.
21. Cornelis F, Tricaud E, Lasserre AS, Petitpierre F, Bernhard JC, Le Bras Y, *et al*. Routinely performed multiparametric magnetic resonance imaging helps to differentiate common subtypes of renal tumours. Eur Radiol 2014;24:1068-80.
22. Rosenkrantz AB, Sekhar A, Genega EM, Melamed J, Babb JS, Patel AD, *et al*. Prognostic implications of the magnetic resonance imaging appearance in papillary renal cell carcinoma. Eur Radiol 2013;23:579-87.
23. Campbell N, Rosenkrantz AB, Pedrosa I. MRI phenotype in renal cancer: Is it clinically relevant? Top Magn Reson Imaging 2014;23:95-115.
24. Chandarana H, Rosenkrantz AB, Mussi TC, Kim S, Ahmad AA, Raj SD, *et al*. Histogram analysis of whole-lesion enhancement in differentiating clear cell from papillary subtype of renal cell cancer. Radiology 2012;265:790-8.
25. Sun MR, Ngo L, Genega EM, Atkins MB, Finn ME, Rofsky NM, *et al*. Renal cell carcinoma: Dynamic contrast-enhanced MR imaging for differentiation of tumor subtypes--correlation with pathologic findings. Radiology 2009;250:793-802.
26. Serter A, Onur MR, Coban G, Yildiz P, Armagan A, Kocakoc E. The role of diffusion-weighted MRI and contrast-enhanced MRI for differentiation between solid renal masses and renal cell carcinoma subtypes. Abdom Radiol (NY) 2021;46:1041-52.
27. Outwater EK, Bhatia M, Siegelman ES, Burke MA, Mitchell DG. Lipid in renal clear cell carcinoma: Detection on opposed-phase gradient-echo MR images. Radiology 1997;205:103-7.
28. Low G, Huang G, Fu W, Moloo Z, Girgis S. Review of renal cell carcinoma and its common subtypes in radiology. World J Radiol 2016;8:484-500.
29. Chen Y, Wu N, Xue T, Hao Y, Dai J. Comparison of contrast-enhanced sonography with MRI in the diagnosis of complex cystic renal masses. J Clin Ultrasound 2015;43:203-09.
30. Mühlfeld AS, Lange C, Kroll G, Floege J, Krombach GA, Kuhl C, *et al*. Pilot study of non-contrast-enhanced MRI vs. ultrasound in renal transplant recipients with acquired cystic kidney disease: A prospective intra-individual comparison. Clin Transplant 2013;27:E694-701.
31. Li X, Xiang X, Lin HT. Differential diagnostic value of magnetic resonance diffusion-weighted imaging and apparent diffusion coefficient for renal clear cell carcinoma and non-clear cell carcinoma. Oncol Lett 2023;25:60.